

Imaging backscattering in graphene quantum point contacts

A. Mreńca-Kolasińska and B. Szafran
AGH University of Science and Technology,
Faculty of Physics and Applied Computer Science,
al. Mickiewicza 30, 30-059 Kraków, Poland

We study graphene quantum point contacts and imaging of the backscattering of the Fermi level wave function by potential introduced by a scanning probe. We demonstrate that – in spite of the Klein phenomenon – interference due to the backscattering at a circular n-p junction induced by the probe potential is visible in spatial maps of conductance as functions of the probe position.

Introduction. Quantum point contacts [1, 2] (QPC) are elementary building blocks of quantum transport devices. Transport phenomena for the current injected through QPCs are studied with the spatial resolution by the scanning gate microscopy (SGM) [3] – a technique in which a charged tip of the atomic force microscope is used to perturb the potential within the 2DEG, induce the backscattering and alter the conductance. SGM has been used in the studies of graphene-based systems, the QPCs [4] states localized within the constriction [5–7], quantum Hall conditions [8–10], and magnetic focused trajectories [11, 12]. Theoretical studies for the magnetic focusing [13] and imaging snake states [14] have also been performed.

SGM for QPCs in III-V semiconductors resolves interference of the incident and backscattered [15–19] wave functions. In graphene, a strong tip potential induces formation of a local n-p junction [20] instead of depletion of the electron gas as in III-V's. The n-p junctions in graphene are transparent for Fermi level electrons incident normally due to the Klein tunneling [21–24]. Nevertheless as we show below the backscattering induced by the n-p junction formed by the tip induces a clear interference image in the SGM maps with a period of half the Fermi wavelength.

In semiconductor heterostructures with two-dimensional electron gas (2DEG), QPCs can be defined by lateral gates, which narrow the conduction channel for Fermi level electrons [2]. In graphene the channel constriction by external gates is ineffective due to Klein tunneling [25]. Etched constrictions have been studied instead by both experiment [26–29] and theory [30–32]. In bilayer graphene [33–35] it is possible to induce a bandgap by applying a bias between the graphene layers [36–38]. Constrictions on graphene with bilayer inclusions have been produced [10]. We consider both etched [Fig.1(a)] and bilayer patched QPCs [Fig.1(b)]. The spatial conductance oscillation period is the same for both, although the latter are less susceptible to perturbation by defects within the constriction.

Theory We use the atomistic tight-binding Hamiltonian spanned by p_z orbitals, $H = \sum_{\langle i,j \rangle} (t_{ij} c_i^\dagger c_j + h.c.) + \sum_i V(\mathbf{r}_i) c_i^\dagger c_i$, where $V(\mathbf{r}_i)$

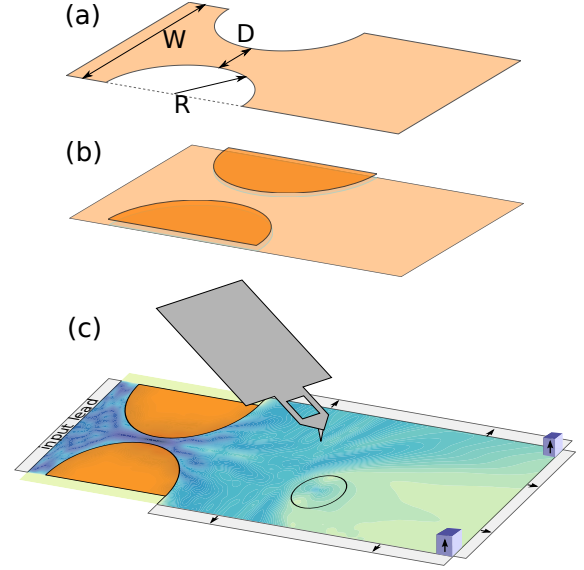


FIG. 1. QPC etched out of graphene (a) and (b) built of patches of bilayer graphene. (c) Schematic drawing of the simulated scanning gate microscopy. The circle indicates the n-p junction for the tip potential equal to the Fermi energy $V = E_F$ is drawn with black line. The light grey lines with the arrows indicate the open boundary conditions introduced as leads. The electric blue blocks with the vertical arrows mark the additional leads used as a sink of currents to absorb backscattering by the corners.

is the external potential at the i -th site at position \mathbf{r}_i , and in the first term we sum over the nearest neighbors. For bilayer patches we assume that the second layer is Bernal (AB) stacked on the first. We use the tight-binding parametrization of Ref. [39] for the intra- and interlayer-hopping parameters (see Supplement). For the simulation of the scanning probe measurement, we assume an effective potential of the tip with a Lorentzian form [40] $V(x, y) = \frac{V_t}{1 + ((x-x_t)^2 + (y-y_t)^2)/d^2}$, where x_t, y_t are the tip coordinates, d is the effective width of the tip potential, and V_t is its maximal value ($V_t = 1.25$ eV unless stated otherwise). For the solution of the quantum scattering problem and evaluation of the transmission probability, we use the wave function matching [41].

We consider an armchair nanoribbon of width $W = 62$ nm, that is 509 atoms wide. The QPC is either formed

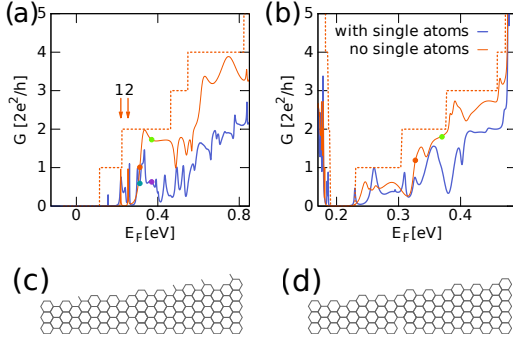


FIG. 2. The conductance of QPCs defined in an armchair nanoribbon of width 509 atoms across the ribbon by etching (a) and bilayer patches (b). The dots mark the workpoints for the conductance mapping (see the text). (c,e) the section of the etched QPC edge with (c) or without (e) single atoms.

by etched out semicircles with radii $R = 28$ nm producing a constriction [Fig. 1(a)] or by bilayer patches of the same form [Fig. 1(b)]. The constriction is $D = 6$ nm wide in the narrowest point. We consider constriction edges with a number of singly connected atoms – similar to the ones present in the Klein edge [42, 43] [Fig. 2(c)] as well as “clean” edges with the singly connected atoms removed [Fig. 2(d)]. For the modeling of SGM experiment, open boundary conditions at the horizontal edges at the output QPC side are applied. We add to the right of the QPC constriction – i.e. the output side – two leads, that are semi-infinite in the y direction and extend all along the upper and lower edge of the nanoribbon [Fig. 1(c)]. The extra leads are introduced to simulate an infinite graphene sheet, which is necessary in order to eliminate the effects of the backscattering from the nanoribbon edges and the subband quantization effects that produce a set of subband-dependent Fermi wavelengths instead of a single one. Upon attachment of the leads, the corners of the computational box – between the right lead and the top or bottom leads [Fig. 1(c)], still act as scattering centers and produce an artificial interference. In order to eliminate the scattering by the corners – which influences the SGM maps – we added in the upper-right and lower-right corners two leads that are semi-infinite in the z -direction, that absorb the current that has not entered the in-plane leads (see Supplement).

Results. In Fig. 2(a) the transmission probability as a function of the Fermi energy is presented. For QPC with singly connected atoms at the etched edge [blue line in Fig. 2(a)], the conductance exhibits a number of sharp peaks. No well-developed plateaux are observed, and the conductance is much lower than the one for a uniform ribbon of the width of the narrowest part of the constriction (dashed line). This is caused by strong backscattering by the atomic-scale roughness of the etched QPC induced by the singly connected atoms. Upon their removal [cf. Fig. 2(c) and 2(d)], the conductance [the or-

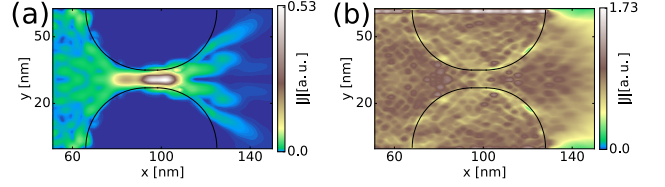


FIG. 3. The current densities in the QPC formed by biased bilayer patches at $E_F = 0.327$ eV (a), within the energy gap of for bilayer patches that is (0.19,0.64) eV. In (b) the Fermi energy $E_F = 0.764$ eV exceeds the bias and current flows across entire ribbon.

ange line in Fig. 2(a)] becomes a smooth function of the energy and approaches the maximal conductance for the constriction width.

For the bilayer patches we assume that the potential on the lower graphene layer is $V = 0$, and V_b on the upper layer. We take $V_b = 0.64$ eV unless stated otherwise. For that bias within the finite size bilayer patches a bandgap is formed in the range of (0.19,0.64) eV. For the Fermi energy inside the bandgap, the current doesn’t penetrate the patches [Fig. 3(a)]. For the Fermi energy beyond the forbidden range the current flows across the patches [Fig. 3(b)]. Similar as the etched QPCs, the geometry of the constriction is specified once the sample is produced, however the bilayer-patched systems can be controlled via the electric field which allows us to turn on and off the quantizing properties, or alter the number of conducting modes in the QPC.

The conductance of the patched QPC is presented in Figure 2(b) as a function of Fermi energy. The dashed line shows the conductance of a uniform nanoribbon with two rectangular bilayer patches along the entire ribbon. There is the ubiquitous backscattering that makes the conductance lower than that of the uniform ribbon of the same structure as the narrowest part of the QPC. With the singly connected atoms the $G(E_F)$ dependence is smoother in the patched QPC [Fig. 2(b)] than for the etched one [Fig. 2(a)] since even for the atoms of the upper layer that have only one neighbor in-plane, there is a non-zero hopping to the atoms in the lower layer.

For modeling the scanning probe experiment the potential of the SGM tip is taken as a Lorentzian (see Methods). For the Fermi energy below the maximum of the induced potential $V_t = 1.25$ eV, the tip introduces an n-p junction. For constrictions without the single-connected atoms we choose the workpoint for the scanning maps at the conductance step ($G \approx G_0$) and at the plateau $G \approx 2G_0$. For the etched QPC the plateau and the step are taken at $E_F = 0.312$ eV ($G = 1.01G_0$, see the orange point in Fig. 2(a)) and $E_F = 0.37$ eV at the etched nanoribbon ($G = 1.73G_0$, see the green point in Fig. 2(a)), respectively. For the patched QPC we take $E_F = 0.37$ for the plateau ($G = 1.8G_0$, see the green point in Fig. 2(b)) and $E_F = 0.327$ eV for the step

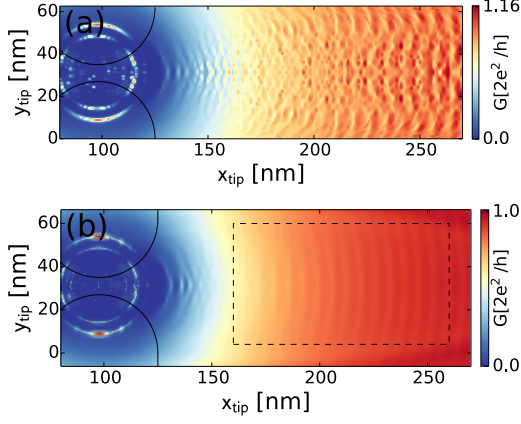


FIG. 4. The conductance of an etched QPC without the singly connected atoms for $E_F = 0.312$ eV [orange dot in Fig. 1(a)] as a function of the SGM tip position for (a) 509 atom wide nanoribbon at the right QPC side (closed boundary conditions at the vertical edges) and (b) an infinite graphene halfplane simulated with open boundary conditions.

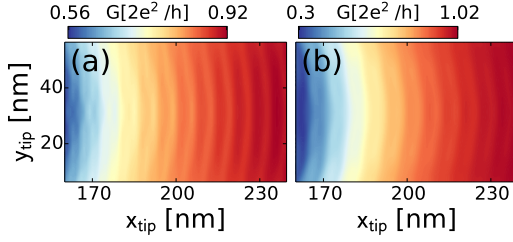


FIG. 5. Map of conductance within the region marked by the dashed rectangle in Fig. 4 for (a) etched and (b) patched QPC. In both cases a clean constriction (patch) edge was taken and a work point with large dG/dE_F was assumed – with $E_F = 0.312$ eV (a) and $E_F = 0.327$ eV (b) – see the orange dots in Fig. 1(a) and 1(b), respectively.

($G = 1.19G_0$, see the orange point in Fig. 2(b)).

For the QPC conductance – in the absence of the tip – the open boundary conditions at the output side of the QPC play no significant role. The conductance is nearly the same with rigid and open boundary conditions for the vertical edges of the ribbon. This fact results from a negligible scattering by the horizontal edges that could reverse the current back through the QPC to the input lead. However, the open conditions are crucial for the conductance mapping.

Let us first consider conductance maps for closed boundary conditions at the upper and lower edge of the ribbon, which are then actual ends of the sample. Fig. 4(a) shows the SGM conductance map for the etched QPC with the clean edge. Away from the constriction in Fig. 4(a) the conductance fluctuates in a non-regular way, due to a large number of transversal modes with different Fermi wave vectors. The nanoribbon of the considered width have 19 modes at the Fermi energy at

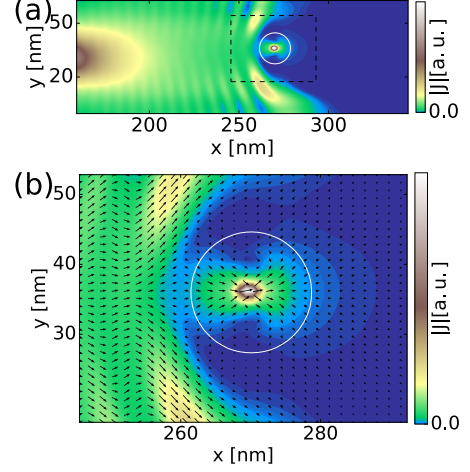


FIG. 6. (a) The current distribution for the etched QPC with the tip located at the axis of the system for the Fermi energy of 0.312 eV. The constriction center is set at $x = 100$ nm. The color map shows the length of the current vector. The white circle shows the n-p junction for $V_t = 1.25$ eV. (b) Zoom of the dashed rectangle in (a) with the current orientation displayed by vectors.

$E_F = 0.312$ eV and 22 modes at $E_F = 0.37$ eV. The image contains the signal of superposition of waves with many different Fermi wavelengths with the intersubband scattering.

The conductance maps become simple once open boundary conditions are applied to the right (output) side of the QPC to simulate an infinite graphene half-plane. In the conductance maps for the etched constriction with open boundary conditions [Fig. 4(b)] the QPC-centered halos remain the same as for the closed boundary conditions [Fig. 4(a)]. The difference occurs to the right of the QPC, where the simulated flake is infinite. Far from the QPC periodic oscillations of conductance are present. Figure 5 shows the zoom at the region [dashed line in Fig. 4(b)] for the etched [Fig. 5(a)] and the patched [Fig. 5(b)] QPC. In both scans the oscillations differ by an offset and not by the oscillations period. The amplitude of the period depends on the $\partial G/\partial E_F$ derivative in Fig. 2. Scans at the conductance steps have higher oscillations amplitude than the ones taken at plateaux (see Supplement).

Discussion. The current distribution for the etched QPC is displayed in Fig. 6 with the interference fringe pattern between the QPC and the tip that results from the tip-induced backscattering. The white circle in Fig. 6 indicates the position where the effective tip potential equals the Fermi energy, i.e. the n-p junction. In Fig. 6(b) a zoom of the rectangle marked in Fig. 6(a) is displayed with the current orientation given by the vector map.

In the Klein tunneling effect the Fermi electron incident on a perpendicular barrier larger than E_F is per-

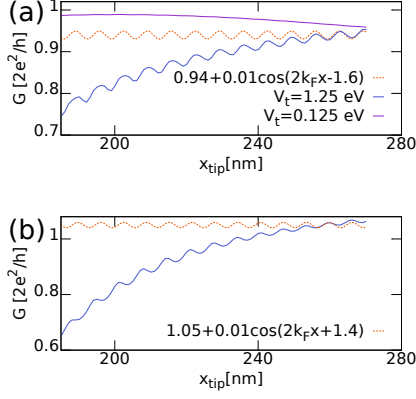


FIG. 7. The blue lines show the cross-sections of the conductance maps along the symmetry axis of the device. (a) corresponds to Fig. 5(a) for an etched QPC with $E_F = 0.312$ eV, and (b) to Fig. 5(b) for a patched QPC with $E_F = 0.327$ eV. The dashed lines indicate the cosine with the Fermi wave vector k_F . From Eq. (2) we find $k_F = 0.4695$ 1/nm for $E_F = 0.312$ eV (a) and $k_F = 0.493$ 1/nm for $E_F = 0.327$ eV (b).

fectly transmitted for normal incidence angle, and the transmission probability is less than 1 for other incidence angles [21, 22]. For a non-normal incidence, the current is partially reflected, and partially transmitted and refracted by the n-p-n junction [44, 45]. In Fig. 6 a normal current along the axis of the system indeed passes across the junction. The tip potential deflects the currents inside the central p conductivity region, and only the precisely normal component of the current passes through undeflected. Other incidence angles contribute to backscattering.

The angular dependence of the scattering by a circular potential in graphene has been described for an incident plane wave in Ref. [45]. In our case the wave function incoming from the QPC opening is not a plane wave but it is closer to a circular wave, which contributes to a deviation of the incidence angles from normal. Moreover, the tip potential that is of an electrostatic origin is bound to possess a smooth profile. According to Ref. [23], for smooth potential profile the transmission probability drops deep below 100% already at a low deviation of the incidence angle from normal.

Let us consider a simple model for conductance oscillations far from the QPC. The QPC is a source of a circular wave function and the SGM tip induces backscattering as argued above. The wave function incident from the QPC is partially reflected back to the opening. The incident wave $\Psi_{in}(\mathbf{r}_{tip}) = \exp(i\mathbf{k}_F(\mathbf{r}_{QPC} - \mathbf{r}_{tip}))$ and the wave backscattered by the tip $\Psi_{sc}(\mathbf{r}_{tip}) = \exp(-i\mathbf{k}_F(\mathbf{r}_{QPC} - \mathbf{r}_{tip}))$ superpose and create a standing wave between the tip and the QPC. The electron density modulation can

be described by

$$|\Psi(\mathbf{r}_{tip})|^2 \propto \cos(2\mathbf{k}_F(\mathbf{r}_{tip} - \mathbf{r}_{QPC})). \quad (1)$$

This form of the scattering density gives rise to conduction map that oscillates with the tip position, with a period of $\lambda_F/2$, where the Fermi wave vector is $\lambda_F = \frac{2\pi}{|\mathbf{k}_F|}$. The Fermi vector can be calculated for low energy from the graphene linear dispersion relation [36]:

$$k_F = \frac{2}{3} \frac{E_F}{ta_{CC}}. \quad (2)$$

In Fig. 7 the cross sections along the axis of the system of Fig. 5(a) and 5(b) are shown together with a cosine shifted in phase and offset to adjust to the conductance calculated from the quantum scattering problem. Far from the constriction, the modeled conductance is close to a cosine with the k_F that agrees with the wave vector obtained from the dispersion relation of graphene. As seen in Figs. 4(b) and Fig. 5, far from the constriction the oscillations can be described by a simple model. In Fig. 7 with the purple line we marked the results obtained for $V_t = 0.125$ eV which is below E_F . In this case no backscattered interference pattern is observed. We find that formation of the n-p junction by the tip is a necessary condition for observation of the interference fringes.

Ref. [4] provided a SGM map of a graphene QPC for nominal tip potential set $V_t = -0.5$ eV. The resistance map of this work [4] resolved only the QPC itself and not the interference fringes that were described here. The nominal V_t value given in Ref. [4] is an unscreened parameter, and it is not granted that the screened tip potential was strong enough to induce formation of the n-p junction, since no control of the Fermi energy was demonstrated [4]. Nevertheless, the present work indicates that observation of the spatial maps of the backscattering interference pattern in graphene is not excluded by the Klein tunnelling effect.

Conclusion. We solved the quantum scattering problem for electron wave functions that pass through a QPC constriction formed by an etched channel or biased bilayer patches within an atomistic tight binding approach with open boundary conditions applied to the output side of the QPC. Independent of the QPC type, we find a clear oscillation of conductance maps with the period of half the Fermi wavelength. The finding that the Klein effect does not prevent observation of the standing waves induced by the tip in graphene opens perspectives for experimental determination of the current distribution, current branching by scattering defects, coherence length, etc.

Acknowledgments This work was supported by the National Science Centre (NCN) according to decision DEC-2015/17/B/ST3/01161. The calculations were performed on PL-Grid Infrastructure.

-
- [1] C. Beenakker and H. van Houten, *Solid State Phys.* **44**, 1 (1991).
- [2] B. J. van Wees, H. van Houten, C. W. J. Beenakker, J. G. Williamson, L. P. Kouwenhoven, D. van der Marel, and C. T. Foxon, *Phys. Rev. Lett.* **60**, 848 (1988).
- [3] H. Sellier, B. Hackens, M. F. Pala, M.G., B. S., W. X., L. Desplanque, V. Bayot, and H. S., *Semicond. Sci. Technol.* **26**, 064008 (2011).
- [4] S. Neubeck, L. Ponomarenko, A. Mayorov, S. Morozov, R. Yang, and K. Novoselov, *Physica E* **44**, 1002 (2012).
- [5] M. R. Connolly, K. L. Chiu, A. Lombardo, A. Fasoli, A. C. Ferrari, D. Anderson, G. A. C. Jones, and C. G. Smith, *Phys. Rev. B* **83**, 115441 (2011).
- [6] N. Pascher, D. Bischoff, T. Ihn, and K. Ensslin, *Appl. Phys. Lett.* **101**, 063101 (2012).
- [7] A. G. F. Garcia, M. König, D. Goldhaber-Gordon, and K. Todd, *Phys. Rev. B* **87**, 085446 (2013).
- [8] M. R. Connolly, R. K. Puddy, D. Logoteta, P. Marconcini, M. Roy, J. P. Griffiths, G. A. C. Jones, P. A. Maksym, M. Macucci, and C. G. Smith, *Nano Lett.* **12**, 5448 (2012).
- [9] R. K. Rajkumar, A. Asenjo, V. Panchal, A. Manzin, Á. Iglesias-Freire, and O. Kazakova, *J. Appl. Phys.* **115**, 172606 (2014).
- [10] C. Chua, M. Connolly, A. Lartsev, T. Yager, S. Lara-Avila, S. Kubatkin, S. Kopylov, V. Fal'ko, R. Yakimova, R. Pearce, T. J. B. M. Janssen, A. Tzalenchuk, and C. G. Smith, *Nano Lett.* **14**, 3369 (2014).
- [11] S. Morikawa, Z. Dou, S.-W. Wang, C. G. Smith, K. Watanabe, T. Taniguchi, S. Masubuchi, T. Machida, and M. R. Connolly, *Appl. Phys. Lett.* **107**, 243102 (2015).
- [12] S. Bhandari, G.-H. Lee, A. Kales, K. Watanabe, T. Taniguchi, E. Heller, P. Kim, and R. M. Westervelt, *Nano Lett.* **16**, 1690 (2016).
- [13] M. D. Petrović, S. P. Milovanović, and F. M. Peeters, *Nanotechnology* **28**, 185202 (2017).
- [14] K. Kolasiński, A. Mreńca-Kolasińska, and B. Szafran, *Phys. Rev. B* **95**, 045304 (2017).
- [15] M. A. Topinka, B. J. LeRoy, R. M. Westervelt, S. E. J. Shaw, R. Fleischmann, E. J. Heller, K. D. Maranowski, and A. C. Gossard, *Nature* **410**, 183 (2001).
- [16] B. J. LeRoy, A. C. Bleszynski, K. E. Aidala, R. M. Westervelt, A. Kalben, E. J. Heller, S. E. J. Shaw, K. D. Maranowski, and A. C. Gossard, *Phys. Rev. Lett.* **94**, 126801 (2005).
- [17] M. P. Jura, M. A. Topinka, M. Grobis, L. N. Pfeiffer, K. W. West, and D. Goldhaber-Gordon, *Phys. Rev. B* **80**, 041303 (2009).
- [18] N. Paradiso, S. Heun, S. Roddaro, L. Pfeiffer, K. West, L. Sorba, G. Biasiol, and F. Beltram, *Physica E* **42**, 1038 (2010).
- [19] B. Brun, F. Martins, S. Faniel, B. Hackens, G. Bachelier, A. Cavanna, C. Ulysse, A. Ouerghi, U. Gennser, D. Mailly, S. Huant, V. Bayot, M. Sanquer, and H. Sellier, *Nat. Commun.* **5**, 4290 (2014).
- [20] C. Gutiérrez, L. Brown, C.-J. Kim, J. Park, and P. A.P., *Nat. Phys.* **12**, 1069 (2016).
- [21] M. I. Katsnelson, K. S. Novoselov, and A. K. Geim, *Nat. Phys.* **2**, 620 (2006).
- [22] P. E. Allain and J. N. Fuchs, *Eur. Phys. J. B* **83**, 301 (2011).
- [23] J. Cayssol, B. Huard, and D. Goldhaber-Gordon, *Phys. Rev. B* **79**, 075428 (2009).
- [24] C. Schulz, R. L. Heinisch, and H. Fehske, *Quantum Matter* **4**, 346 (2015).
- [25] R. Yang, L. Huang, Y.-C. Lai, and C. Grebogi, *Phys. Rev. B* **84**, 035426 (2011).
- [26] Y.-M. Lin, V. Perebeinos, Z. Chen, and P. Avouris, *Phys. Rev. B* **78**, 161409 (2008).
- [27] N. Tombros, A. Veligura, J. Junesch, M. H. D. Guimarães, I. J. Vera-Marun, H. T. Jonkman, and B. J. van Wees, *Nat. Phys.* **7**, 697 (2011).
- [28] B. Terrés, L. A. Chizhova, F. Libisch, J. Peiro, D. Jörger, S. Engels, A. Girschik, K. Watanabe, T. Taniguchi, S. V. Rotkin, J. Burgdörfer, and C. Stampfer, *Nat. Commun.* **7**, 11528 (2016).
- [29] A. Kinikar, P. SaiT., S. Bhattacharyya, A. Agarwala, T. Biswas, S. K. Sarker, K. R., M. Jain, V. B. Shenoy, and A. Ghosh, *Nat Nano advance online publication* (2017).
- [30] F. Muñoz Rojas, D. Jacob, J. Fernández-Rossier, and J. J. Palacios, *Phys. Rev. B* **74**, 195417 (2006).
- [31] S. Ihnatsenka and G. Kirczenow, *Phys. Rev. B* **85**, 121407 (2012).
- [32] S. Ihnatsenka and G. Kirczenow, *Phys. Rev. B* **86**, 075448 (2012).
- [33] E. McCann and M. Koshino, *Rep. Prog. Phys.* **76**, 056503 (2013).
- [34] E. McCann, *Phys. Rev. B* **74**, 161403 (2006).
- [35] E. V. Castro, K. S. Novoselov, S. V. Morozov, N. M. R. Peres, J. M. B. L. dos Santos, J. Nilsson, F. Guinea, A. K. Geim, and A. H. C. Neto, *Phys. Rev. Lett.* **99**, 216802 (2007).
- [36] A. H. Castro Neto, F. Guinea, N. M. R. Peres, K. S. Novoselov, and A. K. Geim, *Rev. Mod. Phys.* **81**, 109 (2009).
- [37] F. Xia, D. B. Farmer, Y.-M. Lin, and P. Avouris, *Nano Lett.* **10**, 715 (2010).
- [38] J. Park, S. B. Jo, Y.-J. Yu, Y. Kim, J. W. Yang, W. H. Lee, H. H. Kim, B. H. Hong, P. Kim, K. Cho, and K. S. Kim, *Adv. Mater.* **24**, 407 (2012).
- [39] B. Partoens and F. M. Peeters, *Phys. Rev. B* **74**, 075404 (2006).
- [40] K. Kolasiński and B. Szafran, *Phys. Rev. B* **88**, 165306 (2013).
- [41] K. Kolasiński, B. Szafran, B. Brun, and H. Sellier, *Phys. Rev. B* **94**, 075301 (2016).
- [42] K. He, A. W. Robertson, S. Lee, E. Yoon, G.-D. Lee, and J. H. Warner, *ACS Nano* **8**, 12272 (2014).
- [43] D. J. Klein and L. Bytautas, *J. Phys. Chem. A* **103**, 5196 (1999).
- [44] G.-H. Lee, G.-H. Park, and H.-J. Lee, *Nat. Phys.* **11**, 925 (2015).
- [45] J. Cserti, A. Pályi, and C. Péterfalvi, *Phys. Rev. Lett.* **99**, 246801 (2007).